

BEVDet: High-Performance Multi-Camera 3D Object Detection in Bird-Eye-View

Junjie Huang* Guan Huang Zheng Zhu Dalong Du
PhiGent Robotics

{junjie.huang, zhengzhu}@ieee.org, {guan.huang, dalong.du}@phigent.ai

Abstract

Autonomous driving perceives the surrounding environment for decision making, which is one of the most complicated scenes for visual perception. The great power of paradigm innovation in solving the 2D object detection task inspires us to seek an elegant, feasible, and scalable paradigm for pushing the performance boundary in this area. To this end, we contribute the BEVDet paradigm in this paper. BEVDet is developed by following the principle of detecting the 3D objects in Bird-Eye-View (BEV), where route planning can be handily performed. In this paradigm, four kinds of modules are conducted in succession with different roles: an image-view encoder for encoding feature in image view, a view transformer for feature transformation from image view to BEV, a BEV encoder for further encoding feature in BEV, and a task-specific head for predicting the targets in BEV. We merely reuse the existing modules for constructing BEVDet and make it feasible for multi-camera 3D object detection by constructing an exclusive data augmentation strategy. The proposed paradigm works well in multi-camera 3D object detection and offers a good trade-off between computing budget and performance. BEVDet with 704×256 (1/8 of the competitors) image size scores 29.4% mAP and 38.4% NDS on the nuScenes val set, which is comparable with FCOS3D (i.e., 2008.2 GFLOPs, 1.7 FPS, 29.5% mAP, and 37.2% NDS), while requires just 12% computing budget of 239.4 GFLOPs and runs 4.3 times faster. Scaling up the input size to 1408×512 , BEVDet scores 34.9% mAP and 41.7% NDS, which requires just 601.4 GFLOPs and significantly suppresses FCOS3D by 5.4% mAP and 4.5% NDS. The superiority of BEVDet tells the magic of paradigm innovation.

1. Introduction

2D visual perception has witnessed rapid development in the past few years and emerged some dominant paradigm

*Corresponding author.

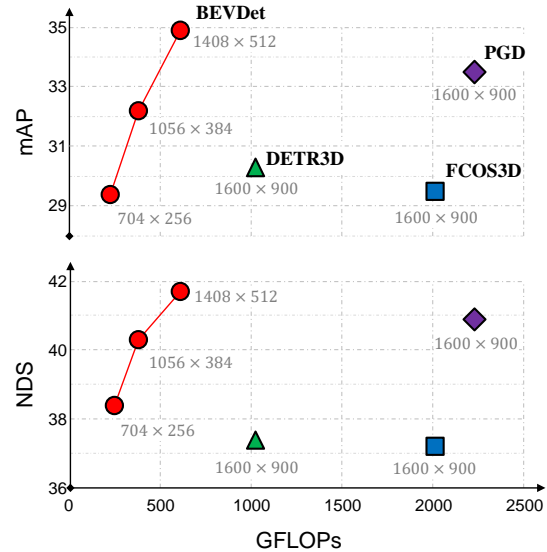


Figure 1: The computing budget and performance of different paradigms on the nuScenes val set.

like Faster R-CNN [33], which is competitive, scalable [10, 2, 4], and task-compatible [10]. However, with respect to the scene of autonomous driving where both performance and time-efficiency are required, the main tasks like 3D object detection and Bird-Eye-View (BEV) semantic segmentation are still conducted by different paradigms in the up-to-date benchmarks. For example, in the nuScenes [1] benchmark, the multi-camera 3D object detection track is dominated by image-view-based methods like FCOS3D [42] and PGD [43], while the BEV semantic segmentation track is dominated by the BEV-based methods like PON [34], Lift-Splat-Shoot [30], and VPN [28]. Which view space is more reasonable for perception in autonomous driving, and can we handle these tasks in a unified view space? Aiming at these questions, we propose BEVDet in this paper. With BEVDet, we explore the feasibility of detecting the 3D object in BEV, expecting a superior performance

compared with the up-to-date image-view-based methods and a consistent paradigm with BEV semantic segmentation. In this way, we can further verify the feasibility of multi-task learning which is meaningful for time-efficient inference.

The proposed BEVDet, as illustrated in Fig. 2, defines and handles the perception problem in the BEV space. It is modularly designed with an image-view encoder for encoding features in image view, a view transformer for transforming the feature from image view into BEV, a BEV encoder for further encoding features in the BEV perspective, and a task-specific head for predicting the targets of the 3D object detection task. Benefiting from this modular design, we can reuse a mass of existing works which have been proved effective in other areas and expect a long way to upgrade this paradigm specific for autonomous driving. We haven't designed any new models in this paper. Instead, we just focus on the feasibility of BEVDet and construct it with some mature works like SwinTransformer [23] for image-view encoder, Lift-Splat-Shoot [30] for view transformer, ResNet [11] for BEV encoder, and CenterPoint [48] for 3D object detection head.

When we start verifying BEVDet, for reasonable performance, the data strategy and the parameter number of BEVDet are set close to the image-view-based 3D object detector like FCOS3D [42] and PGD [43]. Unexpectedly, we encounter a serious overfitting problem. This encourages us to apply a more complicated data augmentation strategy in the image view space as Lift-Splat-Shoot [30] with operations like rotation, scale variation, and random cropping. However, this modification can just partly relieve the overfitting problem when the BEV encoder is absent and even has a negative impact when the BEV encoder is present. We also observe that the view transformer connects the image view space and the BEV space in a pixel-wise manner, and thus, decouples them from the perspective of data augmentation. This makes the data augmentation in image view have no regularization effect on the subsequence modules (*i.e.*, the BEV encoder and the 3D object detection head). Besides, the training data of the image-view encoder is N (*i.e.*, the numbers of cameras like 6 in nuScenes [1]) times that of the subsequence modules. Insufficient training data also push the learning in the BEV space towards overfitting. Base on these observations, we suppose the overfitting problem is dominated by the strong fitting capacity of BEVDet in the BEV space. So, inspired by the LiDAR-based method [48], we apply an extra data augmentation strategy in the BEV space with flipping, scaling, and rotating operations for the model's robustness on these aspects. This works well in preventing BEVDet from overfitting and makes it performs outstandingly on the nuScenes dataset.

As illustrated in Fig. 1, BEVDet achieves competitive

performance (*i.e.*, 29.4% mAP and 38.4% NDS) with an image size of 704×256 , which is merely $1/8$ of the competitors' (*i.e.*, 29.5% mAP and 37.2% NDS with 1600×900 image size in FCOS3D [42]). Scaling down the image size reduces the computing budget to merely 12% and offers a dramatic acceleration of 4.3 times (*i.e.*, BEVDet with 239.4 GFLOPs and 7.3 FPS *v.s.* FCOS3D with 2,000 GFLOPs and 1.7 FPS). By applying a larger image size of 1408×512 , BEVDet scores 34.9% mAP and 41.7% NDS, which has suppressed all existing paradigms with a relatively smaller computing budget of 601.4 GFLOPs and a faster inference speed of 2.3 FPS. Benefiting from explicitly encoding feature in BEV, BEVDet is genius in perceiving the targets' translation, orientation, and velocity.

2. Related Works

2.1. Visual-based 2D Perception

Image Classification The renaissance of deep learning for visual-based 2D perception can be dated back to AlexNet [16] for image classification. From then on, the research community keeps pushing the performance boundary of image encoder by giving raise to residual [11], high-resolution [37], attention-based [6], and many other structures [38, 12, 7, 13, 31]. And at the same time, the powerful image encoding capacity also boosts the performance of other complicated tasks like object detection [33, 20], semantic segmentation [15, 45], human pose estimation [37, 14], and so on. As a simple task, the processing paradigm of image classification is dominated by Softmax [16] and its derivatives. The image encoding capacity determined by the network structure plays a vital role in this problem and is the main concern in the research community.

Object Detection Common object detection, aiming at both classification labels and the instance bounding boxes of all pre-defined objects, is a complicated task where paradigms also play a vital role. Two-stage method FasterRCNN [33], one-stage method RetinaNet [20], and their derivatives [10, 2, 4, 39, 49] are the dominant methods in this area [21, 35]. Inspired by Mask-RCNN [10], multi-task learning has been an appealing paradigm in both the research community and industry community, owing to its great potential for saving computational resources by sharing backbone and promoting tasks by training jointly. The great impact of paradigm innovation in this area inspires us to exploit superior paradigms for better perception performance in the scene of autonomous driving, where the tasks are even more complicated and multi-task learning is rather appealing.

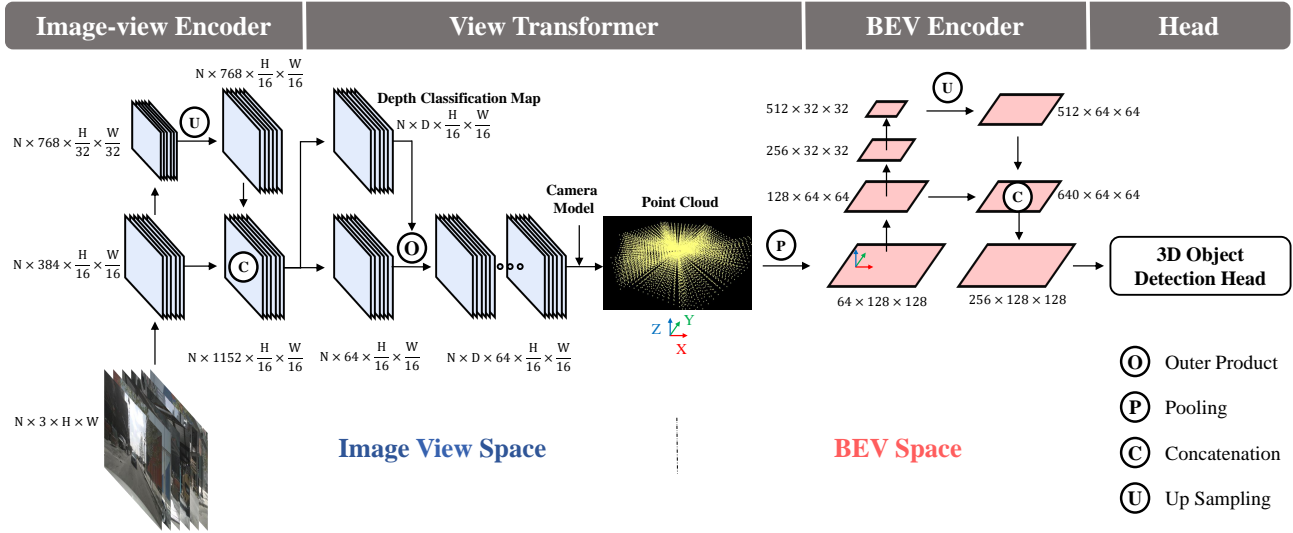


Figure 2: Framework of the proposed BEVDet paradigm. BEVDet with a modular design consists of four modules: Image-view encoder, including a backbone and a neck, is applied at first for image feature extraction. View transformer transforms the feature from the image view to BEV. BEV encoder further encodes the BEV features. Finally, a task-specific head is built upon the BEV features and predicts the target values of the 3D objects. We take BEVDet-STTiny as an example for illustrating the channels of different modules.

2.2. Semantic Segmentation in BEV

One of the main perception tasks in autonomous driving is to construct the maps of the surrounding environment. This can be achieved by semantic segmentation in BEV for the targets like drivable areas, car parking, lane dividers, stopping lines, and so on. The methods with leading performance in benchmark [1] are always with the same perception pipeline [34, 30, 28, 47]. In this pipeline, there are four main components: an image-view encoder for encoding features in image view, a view transformer for transforming the features from image view to BEV, a BEV encoder for further encoding the feature in BEV, and a simple head for pixel-wise classification. The success of this pipeline in BEV semantic segmentation inspires us to extend it to the 3D object detection task, expecting that the features in BEV can work well in capturing some targets of 3D objects like scale and velocity. Besides, we also seek a scalable paradigm where multi-tasks learning can be achieved with both high performance and high efficiency.

2.3. Visual Based 3D Object Detection

3D object detection is another pivotal perception task in autonomous driving. In the last few years, KITTI [8] benchmark has fueled the development of monocular 3D object detection [26, 24, 50, 55, 52, 32, 41, 40, 17]. However, the limited data amount and views make it inappropriate for developing more complicated paradigms. Recently, large-scale benchmark nuScenes [1] is proposed with more

data and multiple views, offering a new perspective toward the paradigm development in multi-camera 3D object detection. Based on this benchmark, some paradigms have been proposed with competitive performance. For example, inspired by the success of FCOS [39] in 2D detection, FCOS3D [42] treats the 3D object detection problem as a 2D object detection problem and conducts perception just in image view. Benefitting from the strong spatial correlation of the targets' attribute with the image appearance, it works well in predicting this but is relatively poor in perceiving the targets' translation, velocity, and depth. Following DETR [3], DETR3D [44] proposes to detect 3D objects in an attention pattern, which achieves similar performance as FCOS3D but with a smaller computing budget and faster inference speed. PGD [43] further develops the FCOS3D paradigm by searching and resolving with the outstanding shortcoming (*i.e.* the prediction of the targets' depth). This offers a remarkable improvement on the baseline but at the cost of more computing budget and larger inference latency. The prominent shortcomings of the existing paradigms encourage us to develop new ones for pushing the performance boundary in this area.

There are some pioneers [32, 18], who have exploited the 3D object detection task in BEV. Among them, also inspired by Lift-Splat-Shoot [30], [32] is the most similar one as ours. They apply the Lift-Spat-Shoot paradigm on monocular 3D object detection and make it competitive in the KITTI [8] benchmark by referring to the LiDAR for the

Module	Component	BEVDet-STTiny	BEVDet-R50	BEVDet-R101
Image-view Encoder	Backbone	SwinTransformer-Tiny	ResNet-50	ResNet-101
	Neck	FPN-LSS-512	FPN-512	FPN-256
View Transformer		Lift-Splat-Shoot-64	Lift-Splat-Shoot-80	Lift-Splat-Shoot-64
BEV Encoder	Layer1	2×Basic-128	2× Basic-160	1× Basic-128
	Layer2	2×Basic-256	2× Basic-320	1× Basic-256
	Layer3	2×Basic-512	2× Basic-640	1× Basic-512
	Neck	FPN-LSS-256	FPN-LSS-256	FPN-LSS-128
Head	CenterPoint Head [48]			

Table 1: BEVDet architecture. ‘-x’ denotes the number of channels in this module.

supervision on depth prediction. A similar idea can also be found in the concurrent work of DD3D [29]. Differently, without the reliance on the LiDAR sensor, we upgrade this paradigm by constructing an exclusive data augmentation strategy based on the decoupling effect of the view transformer. This is a more feasible way and plays a key role in enabling the BEVDet paradigm to perform competitively among existing methods.

3. Methodology

3.1. Network Structure

As illustrated in Fig. 2, BEVDet with a modular design consists of four kinds of modules: an image-view encoder, a view transformer, a BEV encoder, and a task-specific head. We verify the feasibility of BEVDet by constructing 3 derivatives with different structures as listed in Tab. 1. They are all constructed under the principle of containing a similar amount of parameters.

Image-view Encoder The image-view encoder encodes the input images into high-level features. To exploit the power of multi-resolution features, the image-view encoder includes a backbone for high-level feature extraction and a neck for multi-resolution feature fusion. By default, we use the classical ResNet [11] and the up-to-date attention-based SwinTransformer [23] as backbone for prototype study. The substitutions include DenseNet [13], HRNet [37] and so on. With respect to the neck module, we use the classical FPN [19] and the neck structure proposed in [30], which is named FPN-LSS in the following. FPN-LSS simply up-samples the feature with 1/32 input resolution to 1/16 input resolution and concatenates it with the one generated by the backbone with 1/16 input resolution. More complicated neck modules have not been exploited in this paper like PAFPN [22], NAS-FPN [9] and so on.

View Transformer The view transformer transforms the feature from image view to BEV. We apply the view transformer proposed in [30] to construct the BEVDet prototype.

The substitutions include PON [34], VPN [28], PYVA [47], and so on. The adopted view transformer takes the image-view feature as input and densely predicts the depth through a classification manner. Then, the classification scores and the derived image-view feature are used in rendering the predefined point cloud. Finally, the BEV feature can be generated by applying a pooling operation along the vertical direction (*i.e.*, Z coordinate axis as illustrated in Fig. 2).

BEV Encoder The BEV encoder further encodes the feature in the BEV space. Though the structure of this module is similar to that of the image-view encoder with a backbone and a neck, it perceives some pivotal cues like depth, scale, orientation, and speed, which is difficult for predicting in image view. We follow [30] to utilize ResNet [11] with classical residual block to construct the backbone and combine the features with different resolutions by applying FPN-LSS.

Heads The task-specific head is constructed upon the BEV feature. In common sense [1], 3D object detection in automatic pilot aims at the position, scale, orientation, and speed of movable objects like pedestrians, vehicles, barriers, and so on. Without any modification, we directly adopt the 3D object detection head proposed in [48] for prototype verification and fair comparison with the LiDAR-based pipelines like PointPillar [18] and VoxelNet [53].

3.2. Training BEVDet with a Customized Augmentation Strategy

The Isolated View Spaces The adopted view transformer [30] transforms the feature from image view to BEV in a pixel-wise manner. Given a pixel in the image plane $\mathbf{p}_{image} = [x_i, y_i, 1]^T$ with a specific depth d , the corresponding coordinate in the 3D space is:

$$\mathbf{p}_{camera} = I^{-1}(\mathbf{p}_{image} * d) \quad (1)$$

where I is the 3×3 camera intrinsic matrix. Common data augmentation strategies with operations like flipping, cropping, and rotating can be formulated as a 3×3 transforma-

Table 2: Comparison of different paradigms on the nuScenes val set.

Methods	Image Size	#param.	GFLOPs	Modality	mAP \uparrow	mATE \downarrow	mASE \downarrow	mAOE \downarrow	mAVE \downarrow	mAAE \downarrow	NDS \uparrow	FPS
CenterPoint-Voxel [48]	-	-	-	LiDAR	0.564	-	-	-	-	-	0.648	-
CenterPoint-Pillar [48]	-	-	-	LiDAR	0.503	-	-	-	-	-	0.602	-
CenterNet[51]	-	-	-	Camera	0.306	0.716	0.264	0.609	1.426	0.658	0.328	-
FCOS3D [42]	1600 \times 900	52.5M	2,008.2	Camera	0.295	0.806	0.268	0.511	1.315	0.170	0.372	1.7
DETR3D [44]	1600 \times 900	51.3M	1,016.8	Camera	0.303	0.860	0.278	0.437	0.967	0.235	0.374	2.0
PGD [43]	1600 \times 900	53.6M	2,223.0	Camera	0.335	0.732	0.263	0.423	1.285	0.172	0.409	1.4
BEVDet-R50	704 \times 256	53.3M	183.8	Camera	0.286	0.724	0.278	0.590	0.873	0.247	0.372	7.8
BEVDet-R101	704 \times 256	54.1M	223.6	Camera	0.288	0.722	0.269	0.538	0.911	0.270	0.373	7.1
BEVDet-STTiny	704 \times 256	53.7M	215.3	Camera	0.294	0.686	0.278	0.547	0.865	0.261	0.384	7.3
BEVDet-R50	1056 \times 384	53.3M	311.8	Camera	0.304	0.719	0.272	0.555	0.903	0.257	0.381	4.2
BEVDet-R101	1056 \times 384	54.1M	452.0	Camera	0.317	0.704	0.273	0.531	0.940	0.250	0.389	3.8
BEVDet-STTiny	1056 \times 384	53.7M	370.5	Camera	0.322	0.664	0.266	0.508	0.894	0.243	0.403	3.7
BEVDet-STTiny	1408 \times 512	53.7M	601.4	Camera	0.349	0.637	0.269	0.490	0.914	0.268	0.417	2.3

tion matrix A [14]. When a data augmentation strategy is applied on the input image (*i.e.*, $\mathbf{p}'_{image} = A[x_i, y_i, 1]^T$), to maintain the consistency between image pixel and the corresponding points in 3D space, inverse matrix of A should be applied in the view transformation process [30]:

$$\begin{aligned}
\mathbf{p}'_{camera} &= I^{-1}(A^{-1}\mathbf{p}'_{image} * d) \\
&= I^{-1}(A^{-1}A[x_i, y_i, 1]^T * d) \\
&= I^{-1}([x_i, y_i, 1]^T * d) \\
&= \mathbf{p}_{camera}
\end{aligned} \tag{2}$$

As the view transformer connects the two view space in a pixel-wise manner, the augmentation strategy applied in image view space will not change the spatial distribution of the targets in BEV space when Eq. 2 is adopted. This makes performing complicated data augmentation strategies in the image view space feasible for BEVDet.

BEV Space Learning with Data Augmentation. With respect to the learning in the BEV space, the number of data is less than that in the image view space as each sample contains multiple camera images (*e.g.* each sample in the nuScenes benchmark contains 6 images [1]). The learning in the BEV space is thus prone to fall into overfitting. As the view transformer isolates the two view spaces in the augmentation perspective, we construct another augmentation strategy specific for the regularization effect on the learning in BEV space. Common data augmentation operations in 2D space are adopted including flipping, scaling, and rotating. In practice, the operations are conducted both on the output feature of the view transformer and the 3D object detection targets to keep their spatial consistency. It is worth noting that this data augmentation strategy is built upon the precondition that the view transformer can decouple the image-view encoder from the subsequent module. This is a private characteristic of BEVDet and may not be effective in the image-view-based methods, as they project the objects from three-dimensional space into the image view

space. Their targets have a stronger spatial correlation with the input images.

4. Experiment

4.1. Experimental Settings

Dataset We conduct comprehensive experiments on a large-scale dataset, nuScenes [1]. nuScenes dataset includes 1000 scenes with images from 6 cameras with surrounding views, points from 5 Radars and 1 LiDAR. It is the up-to-date popular benchmark for 3D object detection [42, 44, 43, 29] and BEV semantic segmentation [34, 30, 28, 47]. The scenes are officially split into 700/150/150 scenes for training/validation/testing. There are up to 1.4M annotated 3D bounding boxes for 10 classes: car, truck, bus, trailer, construction vehicle, pedestrian, motorcycle, bicycle, barrier, and traffic cone. Following CenterPoint [48], we define the region of interest (ROI) within 51.2 meters in the ground plane with a resolution of 0.8 meters by default.

Evaluation Metrics For 3D object detection, we report the official predefined metrics: mean Average Precision (mAP), Average Translation Error (ATE), Average Scale Error (ASE), Average Orientation Error (AOE), Average Velocity Error (AVE), Average Attribute Error (AAE), and NuScenes Detection Score (NDS). The mAP is analogous to that in 2D object detection [21] for measuring the precision and recall, but defined based on the match by 2D center distance on the ground plane instead of the Intersection over Union (IOU) [1]. NDS is the composite of the other indicators for comprehensively judging the detection capacity. The remaining metrics are designed for calculating the positive results' precision on the corresponding aspects (*e.g.*, translation, scale, orientation, velocity, and attribute).

Training Parameters Models are trained with AdamW [25] optimizer, in which gradient clip is exploited with learning rate $2e-4$, a total batch size of 64 on 8 NVIDIA

Table 3: Comparison with the state-of-the-art methods on the nuScenes test set.

Methods	Modality	mAP \uparrow	mATE \downarrow	mASE \downarrow	mAOE \downarrow	mAVE \downarrow	mAAE \downarrow	NDS \uparrow
PointPillars(Light) [18]	LiDAR	0.305	0.517	0.290	0.500	0.316	0.368	0.453
CenterFusion [27]	Camera & Radar	0.326	0.631	0.261	0.516	0.614	0.115	0.449
CenterPoint [48]	Camera & LiDAR & Radar	0.671	0.249	0.236	0.350	0.250	0.136	0.714
MonoDIS [36]	Camera	0.304	0.738	0.263	0.546	1.553	0.134	0.384
CenterNet [51]	Camera	0.338	0.658	0.255	0.629	1.629	0.142	0.400
FCOS3D [42]	Camera	0.358	0.690	0.249	0.452	1.434	0.124	0.428
PGD [43]	Camera	0.386	0.626	0.245	0.451	1.509	0.127	0.448
BEVDet	Camera	0.398	0.556	0.239	0.414	1.010	0.153	0.463

GeForce RTX 3090 GPUs. For ResNet [11] based image-view encoder, we apply a step learning rate policy, which drops the learning rate at 17 and 20 epoch by a factor of 0.1. With respect to SwinTransformer [23] based image-view encoder, we apply a cyclic policy [46], which linearly increases the learning rate from $2e-4$ to $2e-3$ in the first 40% schedule and linearly decreases the learning rate from $2e-3$ to 0 in the remainder epochs. The total schedule is terminated within 20 epochs.

Data Processing By default in training process, the input images with 1600×900 resolution [1] are processed by random flipping, random scaling with a range of $s \in [0.386, 0.55]$, random rotating with a range of $r \in [-5.4^\circ, 5.4^\circ]$, and finally cropping to 704×256 resolution. The cropping is conduct randomly in the horizon direction but is fixed in the vertical direction (*i.e.*, $(y_1, y_2) = (\max(0, s * 900 - 256), \max(0, s * 900 - 256) + 256)$, where y_1 and y_2 are the upper bound and lower bound of the cropping area.) In the BEV space, the input feature and 3D object detection targets are augmented by random flipping, random rotating with a range of $[-22.5^\circ, 22.5^\circ]$, and random scaling with a range of $[0.95, 1.05]$. Following CenterPoint [48], all models are trained with CBGS [54]. In testing time, the input image is scaled by factor of 0.48 and cropped to 704×256 resolution with a region of $(x_1, x_2, y_1, y_2) = (32, 736, 176, 432)$.

Inference Speed We conduct all experiments based on MMDetection3D [5]. The inference speed is the average upon 6019 validation samples [1]. For monocular paradigms like FCOS3D [42] and PGD [43], the inference speeds are divided by a factor of 6 (*i.e.* the number of images in a single sample [1]), as they take each image as an independent sample. It is worth noting that, the dividing operation may not be the optimal method, as processing in the batch pattern can speed up the inference of monocular paradigms. We suppose the computing budget is a more appropriate perspective for autonomous driving. All inference speeds and computing budgets are tested without data augmentation.

4.2. Benchmark Results

4.2.1 nuScenes val set

We comprehensively compare the proposed BEVDet with other paradigms like FCOS3D [42], its upgraded version PGD [43], and DETR3D [44]. Their numbers of parameters, computing budget, inference speed, and performance on the nuScenes val set are all listed in Tab. 2. We set the number of parameters of BEVDet close to competitors and test BEVDet with different input resolutions including 704×256 , 1056×384 , and 1408×512 .

With merely 1/8 input size of the competitors (*i.e.*, 704×256 for BEVDet *v.s.* 1600×900 for FCOS3D, DETR3D, and PGD), BEVDet requires just 239.4 GFLOPs computing budget, can be processed in 7.3 samples per second, and scores 29.4% mAP and 38.4% NDS. It has a similar mAP performance as FCOS3D (29.5% mAP) and DETR3D (30.3% mAP) while requires far less computing budget (2,008.2 GFLOPs of FCOS3D, 1,016.8 GFLOPs of DETR3D), faster inference speed (1.7 FPS of FCOS3D, 2.0 FPS of DETR3D), and better performance on the composite indicator (37.2% NDS of FCOS3D, 37.4% NDS of DETR3D). BEVDet-1408 \times 512 with 1/2 input size of the competitors requires 601.4 GFLOPs, can be processed in 2.2 FPS, and scores 34.9% mAP and 41.7% NDS. This configuration has suppressed all existing methods including PGD by 0.6% mAP and 1.0% NDS (*i.e.*, the upgraded version of FCOS3D with more computing budget of 2,223.0 GFLOPs, slower inference speed of 1.4 FPS, but better performance of 33.5% mAP and 40.9% NDS). It is worth noting that BEVDet is potentially compatible with the method proposed in PGD. However, their combination is not the scope of this paper and will be studied in future works.

Considering the translation (ATE), scale (ASE), orientation (AOE), velocity (AVE), and attribute (AAE) error of the truly positive results, BEVDet works well in predicting translation, orientation, and velocity, which agrees with common sense that it is easier for an agent to capture these kinds of information in BEV. On the other hand, BEVDet performs poorly in predicting attributes than the image-view-based methods like FCOS3D and PGD. We suppose that the appearance cues are damaged during the transfor-

Table 4: Results of ablation study on the nuScenes `val` set. IDA denotes Image-view-space Data Augmentation. BDA denotes BEV-space Data Augmentation. BE denotes BEV Encoder. The cropping strategy in vertical direction is $(y_1, y_2) = (s * 900 - 256, s * 900)$, which is different from the default setting.

Methods	IDA	BDA	BE	mAP-best \uparrow	NDS-best \uparrow	mAP \uparrow	NDS \uparrow	mATE \downarrow	mASE \downarrow	mAOE \downarrow	mAVE \downarrow	mAAE \downarrow	#param.	GFLOPs	FPS
FCOS3D						0.295	0.372	0.806	0.268	0.511	1.315	0.170	52.5M	2,008.2	1.7
A			\checkmark	0.205(e11)	0.305(e18)	0.184	0.298	0.730	0.291	0.690	1.077	0.233	53.3M	183.8	7.8
B	\checkmark		\checkmark	0.185(e15)	0.281(e11)	0.175	0.274	0.762	0.344	0.708	1.171	0.325	53.3M	183.8	7.8
C		\checkmark	\checkmark	0.259(e18)	0.354(e18)	0.256	0.349	0.744	0.279	0.601	0.937	0.229	53.3M	183.8	7.8
D	\checkmark	\checkmark	\checkmark	-	-	0.284	0.369	0.733	0.279	0.569	0.905	0.241	53.3M	183.8	7.8
E				0.221(e17)	0.309(e18)	0.215	0.306	0.777	0.283	0.703	1.111	0.249	27.8M	125.7	8.0
F	\checkmark			-	-	0.246	0.311	0.796	0.284	0.783	1.130	0.260	27.8M	125.7	8.0
G	\checkmark	\checkmark		-	-	0.267	0.333	0.775	0.280	0.638	1.081	0.309	27.8M	125.7	8.0
G-R101	\checkmark	\checkmark		-	-	0.275	0.347	0.740	0.276	0.607	1.106	0.284	45.9M	206.0	7.3

mation from image view into BEV.

The input size has a large impact on the performance and BEVDet with 1408×512 input size has a 5% mAP superiority on that with 704×256 input size. It is worth noting that with the increase of input size, the scale of the BEVDet computing budget is not a quadratic of the input size variance (*i.e.*, 704×256 with 239.4 GFLOPs *v.s.* 1408×512 ($\times 4$) with 601.4 GFLOPs ($\times 1.88$)), as the computing budget of the BEV encoder and heads is consistent. Besides, a larger input size has a negative impact on the velocity prediction, which is consistent among different backbones.

4.2.2 nuScenes test set

For the nuScenes `test` set, we construct BEVDet with SwinTransformer-Small backbone in image-view encoder. The input image size is set to 2112×768 . The computing budget increases to 2151.0 GFLOPs, which is close to the existing works like PGD [43] and FCOS3D [42]. We adopt a single model with test time augmentation. As listed in Tab. 3, BEVDet peaks on the nuScenes vision-based 3D objection leaderboard¹ with scores of 39.8% mAP and 46.3% NDS, suppressing the previous leading method PGD [43] by 1.2% mAP and 1.5% NDS. It is worth noting that the performance of vision-based BEVDet on composite indicator NDS has exceeded the classical LiDAR-based method PointPillars [18] (*i.e.* 30.5% mAP and 45.3% NDS), showing the feasibility and great potential of vision-based 3D object detection.

4.3. Ablation Studies

With a ResNet-based image-view encoder and an input size of 704×256 , we study how the performance of BEVDet is developed. In this process, some key factors play pivotal roles including Image-view-space Data Augmentation (IDA), BEV-space Data Augmentation (BDA), and BEV Encoder (BE). We compare the performance of different configurations in Tab 4. The evolution of loss,

¹<https://www.nuscenes.org/object-detection>

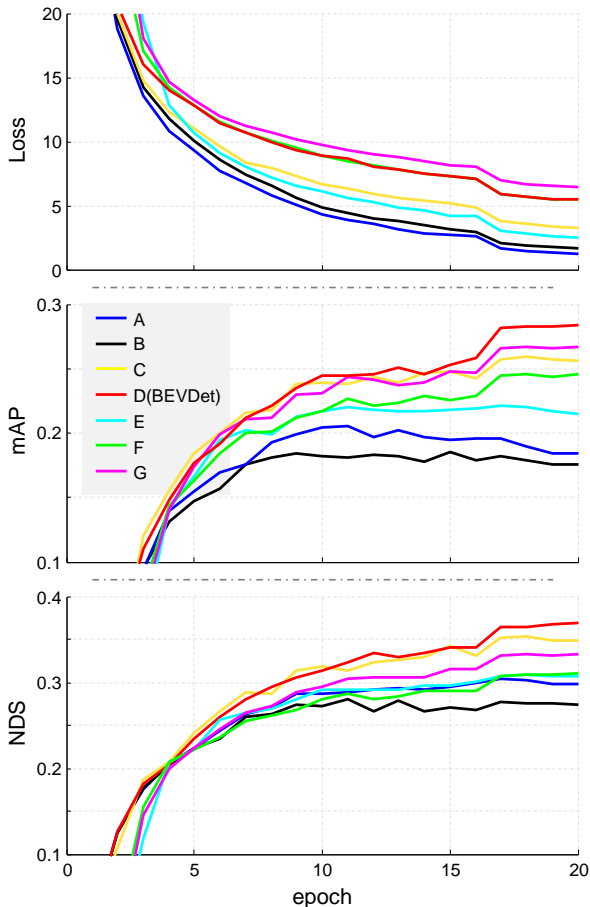


Figure 3: The evolution of loss, mAP, and NDS in the training process. The configurations are defined in Tab 4.

mAP, and NDS in the training process are illustrated in Fig. 3.

As a baseline, we simply replace the BEV feature in LiDAR-based method CenterPoint [48] with the one generated by the view transformer proposed in [30]. In this configuration (A), all augmentation strategies are absent.

During the training process, indicator mAP peaks at epoch 11 and falls into overfitting in the following epochs. Finally, the performance of the convergence is just 18.4% mAP. The performance of this configuration is far poor than the image-view-based method FCOS3D (29.5% mAP).

By merely applying Image-view-space Data Augmentation (IDA), the mAP performance of configuration B peaks at epoch 15 (18.5%) and finally scores 17.5%. The performance of this configuration is even worse than the baseline (A). In contrast, configuration C with BEV-space Data Augmentation (BDA) peaks at epoch 15 with 25.9% mAP and finally scores 25.6% mAP at epoch 20, which suppresses the baseline (A) by a large margin of 7.2% mAP. **BDA plays a more important role than IDA in training BEVDet.** By applying both IDA and BDA in configuration D, the mAP performance peaks at epoch 20 to 28.4%. **IDA has a negative impact on the performance when BDA is absent but has a positive impact when BDA is present.**

To study the impact of BEV Encoder (BE), we remove BE in configuration E, F, and G. The number of parameters drops by 48% from 53.3M to 27.8M. Comparing configuration G with D, BE boosts the BEVDet’s performance by 1.7% mAP, indicating that it is one of the key components in constructing the performance of BEVDet. By comparing configuration E, and F, we found that **IDA can offer a positive impact when BE is absent, which is on the contrary when BE is present.** We suppose that the strong perception capacity of BE can only be built upon the presence of BDA. In configuration G-R101, we replace the backbone of configuration G with ResNet-101, which is 2 times in depth. This configuration scores 27.5% mAP with a larger computing budget of 206.0 GFLOPs. Compared with configuration G, the gains are 0.8% mAP. **Scaling up the image encoder with ResNet-101 backbone is a suboptimal manner when compared with configuration D.**

With respect to the translation, scale, orientation, velocity, and attribute of the positive results, it is worth noting that **IDA has a negative impact on predicting targets’ attributes** (e.g., comparing configuration B with A, D with C, and F with E). **BE has a positive impact on predicting the target’s attribute when IDA is absent** (e.g., comparing configuration A with E and D with G). **BDA has a positive impact on predicting targets’ velocity, scale, and orientation** (e.g., comparing configuration D with B, C with A, and G with E).

Backbone Type of the Image-view Encoder As listed in Tab. 2, when changing the backbone type of the image-view encoder from ResNet-R50 [11] into SwinTransformer-Tiny [23], the gains are 0.8% mAP and 1.2% NDS (i.e., BEVDet-R50 with 28.6% mAP and 37.2% NDS v.s. BEVDet-STTiny with 29.4% mAP and 38.4% NDS). BEVDet-R50 is particularly stronger in predicting the targets’ attributes,

Table 5: Ablation study on the learning rate policies.

Backbone	Schedule	mAP \uparrow	NDS \uparrow
BEVDet-R50	Step	0.286	0.372
BEVDet-R50	Cyclic [46]	0.268	0.342
BEVDet-STTiny	Step	0.292	0.384
BEVDet-STTiny	Cyclic [46]	0.294	0.384

while BEVDet-STTiny has superior performance in predicting the target’s translation, orientation, and velocity. With respect to BEVDet-R101, the gains are merely 0.2% mAP and 0.2% NDS on BEVDet-R50 when a small input size of 704×256 is adopted. However, the gains are 1.3% mAP and 0.8% NDS when a larger input size of 1056×384 is applied. This indicates that a larger receptive field plays an important role in scaling up the input size.

Learning Rate Policy We merely test two kinds of learning rate policies: step and cyclic [46]. As listed in Tab. 5, step policy works better than cyclic when ResNet-50 is adopted as the backbone of the image-view encoder. However, with respect to the SwinTransformer-Tiny backbone, the cyclic policy is better.

5. Conclusion

In this paper, we propose BEVDet, a powerful and scalable paradigm specific for multi-camera 3D object detection. BEVDet is constructed by referring to the success of solving BEV semantic segmentation in BEV and is developed by designing an exclusive data augmentation strategy. Different from the previous paradigms in multi-camera 3D object detection, BEVDet undertakes this problem in the Bird-Eye-View and offers superior cost-efficiency. In the large-scale benchmark nuSenses, BEVDet successfully pushes the performance boundary and is particularly good at predicting the targets’ translation, orientation, and velocity. Future works will focus on (1) improving the performance of BEVDet, particularly on targets’ attribute prediction. (2) studying multi-task learning on 3D object detection and BEV semantic segmentation.

References

- [1] Holger Caesar, Varun Bankiti, Alex H Lang, Sourabh Vora, Venice Erin Liong, Qiang Xu, Anush Krishnan, Yu Pan, Giancarlo Baldan, and Oscar Beijbom. nusenes: A multi-modal dataset for autonomous driving. In *Proceedings of the IEEE Conference on Computer Vision and Pattern Recognition*, pages 11621–11631, 2020.
- [2] Zhaowei Cai and Nuno Vasconcelos. Cascade r-cnn: High quality object detection and instance segmentation. *IEEE Transactions on Pattern Analysis and Machine Intelligence*, 2019.

- [3] Nicolas Carion, Francisco Massa, Gabriel Synnaeve, Nicolas Usunier, Alexander Kirillov, and Sergey Zagoruyko. End-to-end object detection with transformers. In *Proceedings of the European Conference on Computer Vision*, pages 213–229. Springer, 2020.
- [4] Kai Chen, Jiangmiao Pang, Jiaqi Wang, Yu Xiong, Xiao-xiao Li, Shuyang Sun, Wansen Feng, Ziwei Liu, Jianping Shi, Wanli Ouyang, et al. Hybrid task cascade for instance segmentation. In *Proceedings of the IEEE Conference on Computer Vision and Pattern Recognition*, pages 4974–4983, 2019.
- [5] MMDetection3D Contributors. MMDetection3D: Open-MMLab next-generation platform for general 3D object detection. <https://github.com/open-mmlab/mmdetection3d>, 2020.
- [6] Alexey Dosovitskiy, Lucas Beyer, Alexander Kolesnikov, Dirk Weissenborn, Xiaohua Zhai, Thomas Unterthiner, Mostafa Dehghani, Matthias Minderer, Georg Heigold, Sylvain Gelly, et al. An image is worth 16x16 words: Transformers for image recognition at scale. In *Proceedings of the International Conference on Learning Representations*, 2020.
- [7] Shanghua Gao, Ming-Ming Cheng, Kai Zhao, Xin-Yu Zhang, Ming-Hsuan Yang, and Philip HS Torr. Res2net: A new multi-scale backbone architecture. *IEEE Transactions on Pattern Analysis and Machine Intelligence*, 2019.
- [8] Andreas Geiger, Philip Lenz, and Raquel Urtasun. Are we ready for autonomous driving? the kitti vision benchmark suite. In *Proceedings of the IEEE Conference on Computer Vision and Pattern Recognition*, 2012.
- [9] Golnaz Ghiasi, Tsung-Yi Lin, and Quoc V Le. Nas-fpn: Learning scalable feature pyramid architecture for object detection. In *Proceedings of the IEEE Conference on Computer Vision and Pattern Recognition*, pages 7036–7045, 2019.
- [10] Kaiming He, Georgia Gkioxari, Piotr Dollár, and Ross Girshick. Mask r-cnn. In *Proceedings of the International Conference on Computer Vision*, pages 2961–2969, 2017.
- [11] Kaiming He, Xiangyu Zhang, Shaoqing Ren, and Jian Sun. Deep residual learning for image recognition. In *Proceedings of the IEEE Conference on Computer Vision and Pattern Recognition*, pages 770–778, 2016.
- [12] Andrew G Howard, Menglong Zhu, Bo Chen, Dmitry Kalenichenko, Weijun Wang, Tobias Weyand, Marco Andreetto, and Hartwig Adam. Mobilenets: Efficient convolutional neural networks for mobile vision applications. *arXiv preprint arXiv:1704.04861*, 2017.
- [13] Gao Huang, Zhuang Liu, Laurens Van Der Maaten, and Kilian Q Weinberger. Densely connected convolutional networks. In *Proceedings of the IEEE Conference on Computer Vision and Pattern Recognition*, pages 4700–4708, 2017.
- [14] Junjie Huang, Zheng Zhu, Feng Guo, and Guan Huang. The devil is in the details: Delving into unbiased data processing for human pose estimation. In *Proceedings of the IEEE Conference on Computer Vision and Pattern Recognition*, pages 5700–5709, 2020.
- [15] Alexander Kirillov, Yuxin Wu, Kaiming He, and Ross Girshick. Pointrend: Image segmentation as rendering. In *Proceedings of the IEEE Conference on Computer Vision and Pattern Recognition*, pages 9799–9808, 2020.
- [16] Alex Krizhevsky, Ilya Sutskever, and Geoffrey E Hinton. Imagenet classification with deep convolutional neural networks. *Advances in Neural Information Processing Systems*, 25:1097–1105, 2012.
- [17] Abhinav Kumar, Garrick Brazil, and Xiaoming Liu. Groomed-nms: Grouped mathematically differentiable nms for monocular 3d object detection. In *Proceedings of the IEEE Conference on Computer Vision and Pattern Recognition*, pages 8973–8983, 2021.
- [18] Alex H Lang, Sourabh Vora, Holger Caesar, Lubing Zhou, Jiong Yang, and Oscar Beijbom. Pointpillars: Fast encoders for object detection from point clouds. In *Proceedings of the IEEE Conference on Computer Vision and Pattern Recognition*, pages 12697–12705, 2019.
- [19] Tsung-Yi Lin, Piotr Dollár, Ross Girshick, Kaiming He, Bharath Hariharan, and Serge Belongie. Feature pyramid networks for object detection. In *Proceedings of the IEEE Conference on Computer Vision and Pattern Recognition*, pages 2117–2125, 2017.
- [20] Tsung-Yi Lin, Priya Goyal, Ross Girshick, Kaiming He, and Piotr Dollár. Focal loss for dense object detection. In *Proceedings of the International Conference on Computer Vision*, pages 2980–2988, 2017.
- [21] Tsung-Yi Lin, Michael Maire, Serge Belongie, James Hays, Pietro Perona, Deva Ramanan, Piotr Dollár, and C Lawrence Zitnick. Microsoft coco: Common objects in context. In *Proceedings of the European Conference on Computer Vision*, pages 740–755. Springer, 2014.
- [22] Shu Liu, Lu Qi, Haifang Qin, Jianping Shi, and Jiaya Jia. Path aggregation network for instance segmentation. In *Proceedings of the IEEE Conference on Computer Vision and Pattern Recognition*, pages 8759–8768, 2018.
- [23] Ze Liu, Yutong Lin, Yue Cao, Han Hu, Yixuan Wei, Zheng Zhang, Stephen Lin, and Baining Guo. Swin transformer: Hierarchical vision transformer using shifted windows. In *Proceedings of the International Conference on Computer Vision*, 2021.
- [24] Zongdai Liu, Dingfu Zhou, Feixiang Lu, Jin Fang, and Liangjun Zhang. Autoshape: Real-time shape-aware monocular 3d object detection. In *Proceedings of the International Conference on Computer Vision*, pages 15641–15650, 2021.
- [25] Ilya Loshchilov and Frank Hutter. Decoupled weight decay regularization. In *Proceedings of the International Conference on Learning Representations*, 2019.
- [26] Yan Lu, Xinzhu Ma, Lei Yang, Tianzhu Zhang, Yating Liu, Qi Chu, Junjie Yan, and Wanli Ouyang. Geometry uncertainty projection network for monocular 3d object detection. In *Proceedings of the International Conference on Computer Vision*, pages 3111–3121, 2021.
- [27] Ramin Nabati and Hairong Qi. Centerfusion: Center-based radar and camera fusion for 3d object detection. In *Proceedings of the IEEE/CVF Winter Conference on Applications of Computer Vision*, pages 1527–1536, 2021.
- [28] Bowen Pan, Jiankai Sun, Ho Yin Tiga Leung, Alex Andonian, and Bolei Zhou. Cross-view semantic segmentation

- for sensing surroundings. *IEEE Robotics and Automation Letters*, 5(3):4867–4873, 2020.
- [29] Dennis Park, Rares Ambrus, Vitor Guizilini, Jie Li, and Adrien Gaidon. Is pseudo-lidar needed for monocular 3d object detection? In *Proceedings of the International Conference on Computer Vision*, pages 3142–3152, 2021.
- [30] Jonah Philion and Sanja Fidler. Lift, splat, shoot: Encoding images from arbitrary camera rigs by implicitly unprojecting to 3d. In *Proceedings of the European Conference on Computer Vision*, pages 194–210. Springer, 2020.
- [31] Ilija Radosavovic, Raj Prateek Kosaraju, Ross Girshick, Kaiming He, and Piotr Dollár. Designing network design spaces. In *Proceedings of the IEEE Conference on Computer Vision and Pattern Recognition*, pages 10428–10436, 2020.
- [32] Cody Reading, Ali Harakeh, Julia Chae, and Steven L Waslander. Categorical depth distribution network for monocular 3d object detection. In *Proceedings of the IEEE Conference on Computer Vision and Pattern Recognition*, pages 8555–8564, 2021.
- [33] Shaoqing Ren, Kaiming He, Ross Girshick, and Jian Sun. Faster r-cnn: Towards real-time object detection with region proposal networks. *Advances in Neural Information Processing Systems*, 28:91–99, 2015.
- [34] Thomas Roddick and Roberto Cipolla. Predicting semantic map representations from images using pyramid occupancy networks. In *Proceedings of the IEEE Conference on Computer Vision and Pattern Recognition*, pages 11138–11147, 2020.
- [35] Shuai Shao, Zeming Li, Tianyuan Zhang, Chao Peng, Gang Yu, Xiangyu Zhang, Jing Li, and Jian Sun. Objects365: A large-scale, high-quality dataset for object detection. In *Proceedings of the International Conference on Computer Vision*, pages 8430–8439, 2019.
- [36] Andrea Simonelli, Samuel Rota Buló, Lorenzo Porzi, Manuel López-Antequera, and Peter Kotschieder. Disentangling monocular 3d object detection. In *Proceedings of the International Conference on Computer Vision*, pages 1991–1999, 2019.
- [37] Ke Sun, Bin Xiao, Dong Liu, and Jingdong Wang. Deep high-resolution representation learning for human pose estimation. In *Proceedings of the IEEE Conference on Computer Vision and Pattern Recognition*, pages 5693–5703, 2019.
- [38] Mingxing Tan and Quoc Le. Efficientnet: Rethinking model scaling for convolutional neural networks. In *Proceedings of the International Conference on Machine Learning*, pages 6105–6114. PMLR, 2019.
- [39] Zhi Tian, Chunhua Shen, Hao Chen, and Tong He. Fcos: Fully convolutional one-stage object detection. In *Proceedings of the International Conference on Computer Vision*, pages 9627–9636, 2019.
- [40] Li Wang, Liang Du, Xiaoqing Ye, Yanwei Fu, Guodong Guo, Xiangyang Xue, Jianfeng Feng, and Li Zhang. Depth-conditioned dynamic message propagation for monocular 3d object detection. In *Proceedings of the IEEE Conference on Computer Vision and Pattern Recognition*, pages 454–463, 2021.
- [41] Li Wang, Li Zhang, Yi Zhu, Zhi Zhang, Tong He, Mu Li, and Xiangyang Xue. Progressive coordinate transforms for monocular 3d object detection. In *Advances in Neural Information Processing Systems*, 2021.
- [42] Tai Wang, Xinge Zhu, Jiangmiao Pang, and Dahua Lin. Fcos3d: Fully convolutional one-stage monocular 3d object detection. *arXiv preprint arXiv:2104.10956*, 2021.
- [43] Tai Wang, Xinge Zhu, Jiangmiao Pang, and Dahua Lin. Probabilistic and geometric depth: Detecting objects in perspective. *arXiv preprint arXiv:2107.14160*, 2021.
- [44] Yue Wang, Vitor Guizilini, Tianyuan Zhang, Yilun Wang, Hang Zhao, and Justin Solomon. Detr3d: 3d object detection from multi-view images via 3d-to-2d queries. *arXiv preprint arXiv:2110.06922*, 2021.
- [45] Tete Xiao, Yingcheng Liu, Bolei Zhou, Yuning Jiang, and Jian Sun. Unified perceptual parsing for scene understanding. In *Proceedings of the European Conference on Computer Vision*, pages 418–434, 2018.
- [46] Yan Yan, Yuxing Mao, and Bo Li. Second: Sparsely embedded convolutional detection. *Sensors*, 18(10):3337, 2018.
- [47] Weixiang Yang, Qi Li, Wenxi Liu, Yuanlong Yu, Yuxin Ma, Shengfeng He, and Jia Pan. Projecting your view attentively: Monocular road scene layout estimation via cross-view transformation. In *Proceedings of the IEEE Conference on Computer Vision and Pattern Recognition*, pages 15536–15545, 2021.
- [48] Tianwei Yin, Xingyi Zhou, and Philipp Krahenbuhl. Center-based 3d object detection and tracking. In *Proceedings of the IEEE Conference on Computer Vision and Pattern Recognition*, pages 11784–11793, 2021.
- [49] Shifeng Zhang, Cheng Chi, Yongqiang Yao, Zhen Lei, and Stan Z Li. Bridging the gap between anchor-based and anchor-free detection via adaptive training sample selection. In *Proceedings of the IEEE Conference on Computer Vision and Pattern Recognition*, pages 9759–9768, 2020.
- [50] Yunpeng Zhang, Jiwen Lu, and Jie Zhou. Objects are different: Flexible monocular 3d object detection. In *Proceedings of the IEEE Conference on Computer Vision and Pattern Recognition*, pages 3289–3298, 2021.
- [51] Xingyi Zhou, Dequan Wang, and Philipp Krähenbühl. Objects as points. *arXiv preprint arXiv:1904.07850*, 2019.
- [52] Yunsong Zhou, Yuan He, Hongzi Zhu, Cheng Wang, Hongyang Li, and Qinhong Jiang. Monocular 3d object detection: An extrinsic parameter free approach. In *Proceedings of the IEEE Conference on Computer Vision and Pattern Recognition*, pages 7556–7566, 2021.
- [53] Yin Zhou and Oncel Tuzel. Voxelnet: End-to-end learning for point cloud based 3d object detection. In *Proceedings of the IEEE Conference on Computer Vision and Pattern Recognition*, pages 4490–4499, 2018.
- [54] Benjin Zhu, Zhengkai Jiang, Xiangxin Zhou, Zeming Li, and Gang Yu. Class-balanced grouping and sampling for point cloud 3d object detection. *arXiv preprint arXiv:1908.09492*, 2019.
- [55] Zhikang Zou, Xiaoqing Ye, Liang Du, Xianhui Cheng, Xiao Tan, Li Zhang, Jianfeng Feng, Xiangyang Xue, and Er-rui Ding. The devil is in the task: Exploiting reciprocal

appearance-localization features for monocular 3d object detection. In *Proceedings of the International Conference on Computer Vision*, pages 2713–2722, 2021.